Dynamical Arrest Transition in Nanoparticle Dispersions with Short-Range Interactions

Aaron P. R. Eberle,[1] Norman J. Wagner,[1] and Ramón Castañeda-Priego[1,2]

[1]*Center for Neutron Science and Department of Chemical Engineering, University of Delaware, Newark, Delaware 19716, USA*
[2]*División de Ciencias e Ingenierías, Universidad de Guanajuato, 37150 León, Mexico*

(Received 6 January 2011; revised manuscript received 10 February 2011; published 11 March 2011)

We measure the dynamical arrest transition in a model, thermoreversible, adhesive hard sphere dispersion. At low volume fractions ϕ, below the critical point, gelation occurs within the gas-liquid phase boundary. For ϕ slightly below and above the critical concentration, the phase boundary follows the predicted percolation transition. At high ϕ, it melds into the predicted attractive-driven glass transition. Our results demonstrate that for ϕ above ~20% physical gelation is an extension of the attractive-driven glass line and occurs without competition for macroscopic phase separation.

DOI: 10.1103/PhysRevLett.106.105704 PACS numbers: 64.70.pv, 64.75.Xc, 82.70.Dd

Colloidal glasses are characterized by a dynamical arrest of the disperse phase and transition out of equilibrium resulting in a loss of ergodicity [1]. For hard spheres, the repulsive-driven glass (RDG) transition is well known to occur at volume fraction $\phi \sim 0.58$ [2]. The addition of a short-range attraction, as in the case of adhesive hard spheres (AHSs), can induce an additional glassy state, an attractive-driven glass (ADG) [3]. While dynamical arrest at high concentrations can be well described with simulation techniques and the mode-coupling theory (MCT), the transition at intermediate ϕ, often termed gelation, is less clear [4]. In the recent literature there has been significant debate on the location of the gel line in relation to the ADG transition and the gas-liquid coexistence region. Recent experiments and simulations have shown that for depletion aggregation gelation is a result of spinodal decomposition such that the gel line intersects the gas-liquid coexistence region to the right of the critical point [5]. Yet it has been shown in model systems, such as the thermoreversible octadecyl silica, that stable gels can form around or below the critical ϕ [6–11]. In support of this, the percolation theory [12] and simulations [13] predict the formation of clusters large enough to span the system without competition for phase separation at low ϕ. Early studies by MCT and Monte Carlo (MC) simulations suggest that gelation is an extension to lower concentrations of the ADG line in a similar manner to percolation [3,14]. However, numerical simulations have shown that previous MCT results overestimate the location of the gel line, suggesting the phase boundary is buried within the coexistence region [4,15]. While the fluid-to-gel phase transition for depletion-driven aggregation has become clearer, it is debatable whether the location of the phase transition is universal to all AHS systems. In this Letter, we directly address this debate by experimentally studying the dynamical arrest transition of a model AHS nanoparticle system ($\Delta = 0.01$, where Δ is the square-well width and in units of σ, the particle diameter). Our results show a continuous boundary that intersects the gas-liquid coexistence region below the critical concentration without competition for phase separation and suggests that gelation is dependent on the physical mechanism of attraction.

In this work, we use the widely studied octadecyl-coated silica particles, synthesized by using the method of van Helden, Jansen, and Vrij [16] and suspended in *n*-tetradecane. The specific details of our particles and their extensive characterization can be found elsewhere [17]. The particle core has a diameter $\sigma = 28.0 \pm 0.1$ nm and polydispersity PD $= 0.10 \pm 0.005$. The dispersion ϕ was calculated based on a combined fractional density of the core and shell and verified by small-angle neutron scattering (SANS). The interparticle potential, and resultant aggregation, is controlled via temperature as a direct manifestation of a fluid-to-solid phase transition of the brush [17]. The brush molecular chain freezing induces a reversible molecular attraction that manifests as short-range attraction between particles.

Measurements were performed for a wide range of dispersion concentrations: $\phi = 0.09 \pm 0.01$ to 0.52 ± 0.01. We define gelation and determine the gel temperature (T_{gel}) to within $\pm 0.1\,^{\circ}$C by using a combination of the classic Winter-Chambon [18] rheological criterion further corroborated with fiber-optic quasielastic light scattering. At T_{gel} we observe a single phase that is stable for weeks. Although the highest ϕ approach the ADG line, we refer to the dynamical arrest transition for all the dispersions as the gel transition within this Letter. SANS is used to probe the nanostructure of the dispersion at and around T_{gel}. Quantitative modeling of the SANS scattering profiles yields the strength of attraction.

Small-amplitude oscillatory shear rheological measurements used to identify the transition from the fluid state to dynamical arrest [18] are shown in Fig. 1. The small-amplitude oscillatory shear results for a temperature ramp experiment for one dispersion, $\phi = 0.12$, can be seen in Fig. 1(a). At high temperatures ($T > \sim 31\,^{\circ}$C), in the fluid state, the suspension exhibits a negligible G', but as the system is quenched the suspension transitions to a

strong viscoelastic solid. For this ϕ the elastic modulus increases over 5 orders of magnitude in the narrow temperature range of 29 °–27 °C. Frequency sweep experiments on the same sample can be seen in the Fig. 1 inset as a function of temperature near the gel point. At the highest temperature shown, 28.4 °C, G'' is larger than G' over the whole frequency range tested. As the temperature is decreased to 28.2 °C, G' and G'' become comparable at high frequencies. At lower temperatures, the sample has a greater elastic modulus, characteristic of solidlike behavior. At 28.2 °C, G' and G'' are nearly equal with power-law slopes of $\frac{1}{2}$, over more than a decade of frequency, which is a characteristic feature of gelation [18]. This rheological feature is consistently observed for all samples and is used to define the gelation temperature. Because this is a physical gel, there is evidence of the expected low frequency relaxation as a deviation from this power-law behavior. However, the sample will support its weight in gravity at this temperature and flow at higher temperatures.

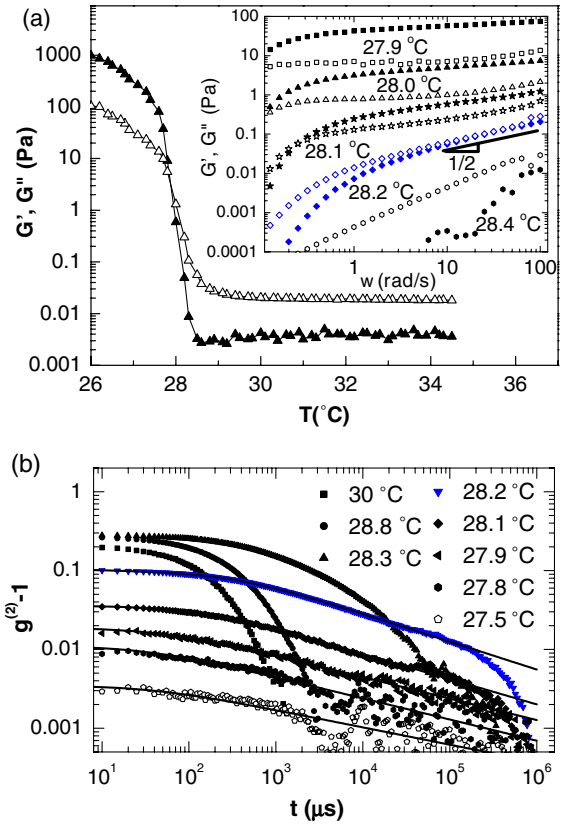

FIG. 1 (color online). (a) Storage G' and loss G'' moduli vs temperature in a small-amplitude oscillatory (stress amplitude $\sigma_o = 17.68$ mPa and frequency $\omega = 2\pi$ rad/s) temperature ramp experiment (ramp rate 0.2 °C/ min). Inset: G' (closed symbols) and G'' (open symbols) from frequency sweep measurements at temperatures around the gel point. The data are offset vertically for clarity by factors 0.03, 0.05, 0.08, and 0.2 for temperatures 28.4°, 28.2°, 28.1°, and 28 °C, respectively. (b) Autocorrelation function vs delay time (scattering angle $\theta = 153°$) as a function of temperature near the gel transition. For all experiments the dispersion $\phi = 0.12$.

The fiber-optic quasielastic light scattering autocorrelation function $g^{(2)} - 1$ vs delay time t for the same dispersion at temperatures near T_{gel} is shown in Fig. 1(b). The autocorrelation function changes from an exponential decay to a power law at 28.2 ± 0.1 °C, which is again a characteristic signature of gelation. Fits of $g^{(2)} - 1$ at and below T_{gel} were performed by using Eq. (10) found in Elliot *et al.* [19] (theory from Martin and Wilcoxon [20]). This leads to a power-law exponent of $n = 0.65 \pm 0.02$ and a corresponding fractal dimension of $d_f = 1.8 \pm 0.05$ [21]. This result agrees with independent measurements of the fractal dimension extracted from SANS experiments where we find $d_f = 1.7 \pm 0.05$. Thus, fiber-optic quasielastic light scattering, SANS, and rheology provide a consistent determination of the gelation temperature.

SANS measurements were performed over a range of temperatures spanning the transition from the fluid state through dynamical arrest. The scattering intensity I versus scattering wave vector Q for a dispersion $\phi = 0.12$ is shown in Fig. 2(a) for varying temperatures. The scattering intensity evolves systematically in the fluid state with decreasing temperature and increasing short-range attraction strength. For temperatures below T_{gel} (28.2 ± 0.1 °C), the scattering profiles overlap and do not significantly change.

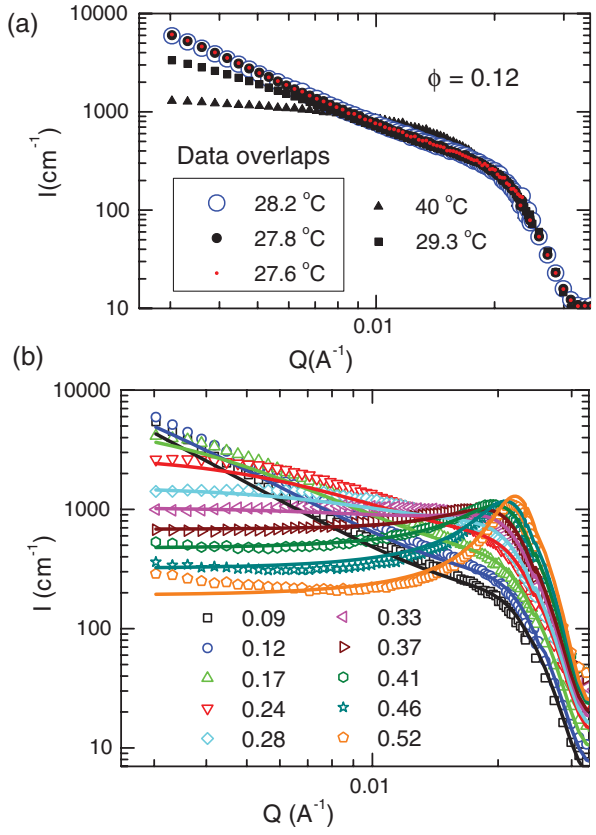

FIG. 2 (color). (a) SANS intensity I versus scattering wave vector Q as a function of temperature for $\phi = 0.12$. (b) SANS measurements at the gel point for various ϕ and the corresponding model fits.

Figure 2(b) shows the SANS spectra at T_{gel}, as identified from rheology, for the entire concentration range.

The scattering intensities in the fluid state and at T_{gel} are compared for three different $\phi = 0.09$, 0.29, and 0.52, in Figs. 3(a)–3(c), respectively. Also shown in Fig. 3 is a visualization of the structure generated via a MC simulation by using the potential extracted from an analysis of the SANS data. The substantial increase in the scattering intensity at low Q, for less-concentrated dispersions, such as in Fig. 3(a), is a direct consequence of the increasing short-range attraction. For increasing concentrations, however, the overall change in $I(Q)$ with temperature decreases. This is because the particulate excluded volume prevents significant spatial rearrangement of the particles at such high ϕ, which can be seen in the MC snapshots. At the highest concentration tested, $\phi = 0.52$, the change in the scattering intensity from the fluid to the arrested state is evident only upon close inspection of the data [see the inset in Fig. 3(c)], which is consistent with a glass transition [9].

The absolute coherent neutron scattering intensity is modeled as $I(Q) = \Omega P(Q) S(Q)$, where Ω is a collection of material constants including the particle volume and ϕ and scattering length density of the dispersion constituents. $P(Q)$ and $S(Q)$ are the form factor and structure factors describing the scattering contributions from a single particle and the interference from the spatial arrangement of the particles, respectively. The particles are accurately modeled by using a polydisperse core-shell form factor [22]. The core and shell characteristics that define all the model parameters for $P(Q)$ are well characterized from independent experiments, as described elsewhere [17].

$S(Q)$ is modeled by using a square-well potential as calculated from the Ornstein-Zernike (OZ) equation with the Percus-Yevick (PY) closure relation [6,7,23]. Comparison between the PY-OZ results and MC simulations show good agreement, as seen in the Fig. 3(a) inset. The range of attraction is characterized by a perturbation parameter $\varepsilon = \Delta/(\sigma + \Delta)$ [24]. For this system $\varepsilon = 0.01$ was used for all concentrations and temperatures as it gave the most accurate description of the scattering profiles and is consistent with previous work [6,9]. Because the model system has been well characterized, this leaves only one unconstrained variable, the square-well depth $U(r)$. The fits of the SANS scattering intensity profiles at T_{gel} can be seen in Fig. 2(b). In the AHS limit, the strength of the interaction is most easily defined by a reduced temperature [24] τ:

$$\tau = \frac{1}{12\varepsilon} \exp\left(\frac{-U(r)}{kT}\right) = \frac{1}{4(B_2^* - 1)}, \qquad (1)$$

where kT is the thermal energy. The mapping between the square-well potential and the AHS potential (an equivalent representation is via the reduced second virial coefficient B_2^* [4,6,7]) is well studied and valid for narrow wells of the order of a few percent of the particle diameter [25]. The values of τ for all dispersions measured at T_{gel} are presented in Fig. 4. As anticipated [25], these results for τ are robust in that all fits with $\varepsilon < 0.1$ gave similar values.

The state diagram with our experimentally determined gel transition for the AHS system is presented in Fig. 4. At intermediate to low ϕ and high attractive strength, there is a liquid-vapor coexistence region. Conversely, at high ϕ

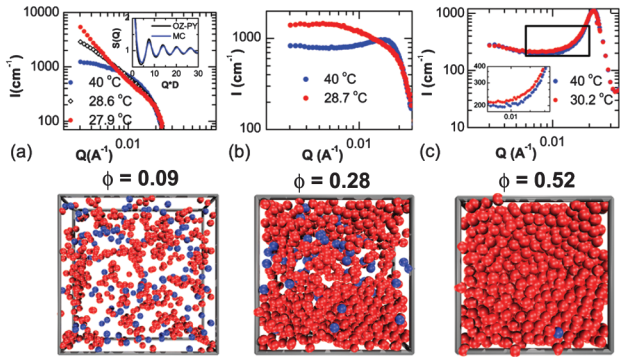

FIG. 3 (color). Comparison of the SANS scattering profile for the nanoparticle dispersion at temperatures in the fluid and gel state for three ϕ: (a) 0.09, (b) 0.28, and (c) 0.52; the inset is an expanded image of the outlined box. The inset in (a) depicts the structure factor $S(Q)$ calculated by using the Ornstein-Zernike equation with the Percus-Yevick closure relation (OZ-PY) and a MC simulation for an ideal population of monodisperse spheres with the interaction potential parameters extracted from the SANS data. The simulated structure at each ϕ gives a qualitative depiction of the gel structure where the red and blue spheres represent the bonded and unbonded nanoparticles, respectively. The cartoons show a slice of the total simulation box, 6 particle diameters thick.

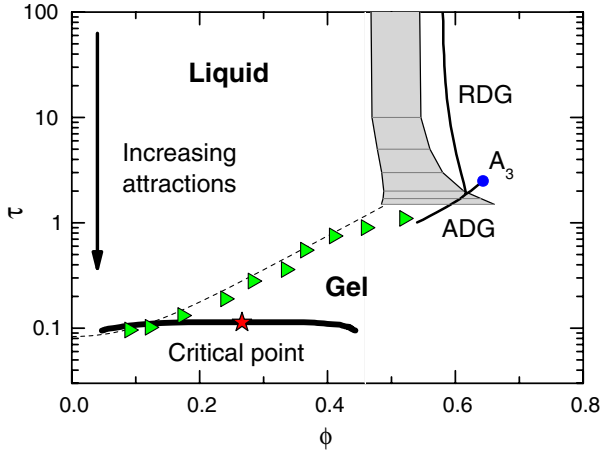

FIG. 4 (color online). State diagram for the model AHS system. The solid line is the liquid-vapor coexistence region with a critical point (star, $\tau = 0.1133$, and $\phi = 0.266$) as determined by MC simulations [28]; the broken line is the analytical solution to the percolation line [12]; the gray shaded region is the liquid-crystal coexistence region from the modified weighted-density approximation theory [29]; the solid lines are RDG and ADG lines from the MCT with point singularity A_3 (circle) [3]. The triangles are the experimentally determined dynamical arrest transition.

and low attractive strength, there is a liquid-crystal coexistence region. This is in addition to a RDG line which intersects the ADG line with mode-coupling theory singularity A_3. As is typically done, the location of the RDG and ADG lines calculated from the MCT are shifted to higher particle densities by using known experimental data, as the MCT underpredicts the RDG line [2,3]. The percolation line for the AHS fluid can be seen extending from the liquid-vapor coexistence region at low ϕ to the liquid-crystal coexistence region at high ϕ. The experimentally determined points of dynamical arrest (triangles) agree well with the percolation theory up to $\phi \sim 0.41$. For concentrations $\phi > \sim 0.41$ the boundary for dynamical arrest tends toward and joins the ADG line. Thus, the major conclusions of this work show that, for this AHS nanoparticle system, the dynamical arrest transition extends from the dilute particle concentration side of the liquid-vapor coexistence above the critical point following predictions of the percolation theory until at sufficiently high particle concentrations it subtends the predictions and joins the MCT ADG line.

These results differ quantitatively from prior published results by Verduin and Dhont [6], and Grant and Russel [7], who used a similar system. The results differ because of differences in the definition of the gel line, the method to determine the strength of attraction, and in the suspending medium. The temperature of dynamical arrest corresponding to the gel transition is defined by Verduin and Dhont as the point where the observed speckle pattern of scattered light becomes static in a light scattering experiment. From Fig. 1(b), we can see that this will lead to a lower temperature than the point of percolation. In addition, the authors used a different suspending medium, which changes the molecular mechanism responsible for particle attraction [26]. In the work of Grant and Russel, the strength of attraction was determined by fitting the low-Q static light scattering results in the fluid region to a linear function of temperature and extrapolating to T_{gel}. This approach led to an even lower τ. We believe that our use of multiple, corroborative methods to define the temperature of dynamical arrest (T_{gel}) and our quantitative modeling of the entire SANS spectra over a wide concentration range provides a more accurate determination of the AHS gel transition.

The location of the liquid-vapor coexistence boundary has been shown to depend on the shape and range of the attractive potential [4,24,25]. However, for all reasonably narrow attractive interactions, when mapped on the state diagram variables our dynamical arrest transition intersects the phase boundary below the critical concentration. In addition, the RDG and ADG lines vary in location depending on the potential and level of approximation [3,27]. Again, however, when plotted on this state diagram, our measurements of the dynamical arrest line are in the close vicinity of the ADG for concentrated dispersions with short-range attractions. We anticipate that improvements to the theory and to the rheological and dynamical criteria that identify the dynamical arrest transition may refine the location of the various boundaries in the AHS state diagram. However, the connection between the dilute and concentrated states of dynamical arrest is defined experimentally by the measurements presented herein.

We thank Paul Butler, Yun Liu, Steve Kline, Wilson Poon, Jan Dhont, Johan Bergenholtz, and Jan Vermant for valuable discussions. The funding for this work was provided by the NIST Cooperative Agreement No. 70NANB7H6178. This work utilized facilities supported in part by the National Science Foundation under Agreement No. DMR-0454672.

[1] W. C. K. Poon, A. D. Pirie, and P. N. Pusey, Faraday Discuss. **101**, 65 (1995).
[2] P. N. Pusey and W. van Megen, Phys. Rev. Lett. **59**, 2083 (1987).
[3] J. Bergenholtz and M. Fuchs, Phys. Rev. E **59**, 5706 (1999).
[4] E. Zaccarelli, J. Phys. Condens. Matter **19**, 323101 (2007).
[5] P. J. Lu *et al.*, Nature (London) **453**, 499 (2008).
[6] H. Verduin and J. K. G. Dhont, J. Colloid Interface Sci. **172**, 425 (1995).
[7] M. C. Grant and W. B. Russel, Phys. Rev. E **47**, 2606 (1993).
[8] M. J. Solomon and P. Varadan, Phys. Rev. E **63**, 051402 (2001).
[9] M. Sztucki *et al.*, Phys. Rev. E **74**, 051504 (2006).
[10] H. Hoekstra *et al.*, Langmuir **21**, 11 017 (2005).
[11] R. Vavrin *et al.*, J. Chem. Phys. **130**, 154903 (2009).
[12] Y. C. Chiew and E. D. Glandt, J. Phys. A **16**, 2599 (1983).
[13] W. G. T. Kranendonk and D. Frenkel, Mol. Phys. **64**, 403 (1988).
[14] G. Foffi *et al.*, Phys. Rev. E **65**, 031407 (2002).
[15] G. Foffi *et al.*, Phys. Rev. Lett. **94**, 078301 (2005).
[16] A. K. van Helden, J. W. Jansen, and A. Vrij, J. Colloid Interface Sci. **81**, 354 (1981).
[17] A. P. R. Eberle *et al.*, Langmuir **26**, 3003 (2010).
[18] H. H. Winter and F. Chambon, J. Rheol. **30**, 367 (1986).
[19] S. L. Elliott *et al.*, Faraday Discuss. **123**, 369 (2003).
[20] J. E. Martin and J. P. Wilcoxon, Phys. Rev. Lett. **61**, 373 (1988).
[21] W. Hess, T. A. Vilgis, and H. H. Winter, Macromolecules **21**, 2536 (1988).
[22] S. R. Kline, J. Appl. Crystallogr. **39**, 895 (2006).
[23] A. Woutersen and C. G. Dekruif, J. Chem. Phys. **94**, 5739 (1991).
[24] S. V. G. Menon, C. Manohar, and K. S. Rao, J. Chem. Phys. **95**, 9186 (1991).
[25] M. G. Noro and D. Frenkel, J. Chem. Phys. **113**, 2941 (2000).
[26] S. Roke *et al.*, J. Phys. Condens. Matter **17**, S3469 (2005).
[27] K. N. Pham *et al.*, Science **296**, 104 (2002).
[28] M. A. Miller and D. Frenkel, Phys. Rev. Lett. **90**, 135702 (2003).
[29] D. W. Marr and A. P. Gast, J. Chem. Phys. **99**, 2024 (1993).